scientific reports

Check for updates

OPEN

A pre-clinical MRI-guided all-in-one focused ultrasound system for murine brain studies

Tarana Parvez Kaovasia[1]✉, Sarah Duclos[1], Dinank Gupta[1], Kourosh Kalayeh[2], Mario Fabiilli[2], Douglas C. Noll[1,2], Jonathan Sukovich[1], Aditya Pandey[3], Zhen Xu[1,2,3] & Timothy L. Hall[1]

This paper describes the design and initial proof-of-concept of a single pre-clinical transcranial focused ultrasound (FUS) system capable of performing histotripsy (mechanical ablation), hyperthermia, blood-brain barrier opening (BBBO), sonodynamic therapy, or neuromodulation in a murine brain. We have termed it the All-in-One FUS system for murine brain studies, which is the first FUS system of its kind. The 1.5 MHz ultrasound transducer was fabricated and driven using a custom electronic driver to produce 3-cycle pulses with a focal peak-negative pressure (P-) of up to 87 MPa at a low duty cycle (< 0.1%) for histotripsy as well as 50% duty cycle pulsed-ultrasound with a spatial-peak temporal-average intensity (I_{spta}) of up to 251 W/cm^2 for the other FUS modalities. This All-in-One system can be guided by MRI or stereotactically to maximize its flexibility. To validate the design of the system, histotripsy, BBBO, and hyperthermia were performed in naïve brains of two mice for each modality. Histotripsy and BBBO were performed using MRI-based stereotactic co-registration. The therapeutic effect was confirmed using T2-weighted MR-images for histotripsy, and T1-weighted Gadolinium contrast-enhanced MR-images for BBBO. For hyperthermia, an MRI-compatible insert was designed to fit inside the 80 mm imaging coil of a 7-Tesla small-animal MRI-system, with T2-weighted MR-images used to confirm targeting, and MR-thermometry used to monitor the thermal dose delivered.

Keywords Therapeutic ultrasound, Brain, Histotripsy, Blood-brain barrier opening, Hyperthermia, Magnetic resonance imaging (MRI)

Focused Ultrasound (FUS) is a non-invasive therapeutic modality that has been gaining rapid momentum in the treatment of a multitude of brain diseases like brain tumors[1,2], stroke[3,4], essential tremor[5,6], Parkinson's disease[7], and Alzheimer's disease[8–10]. FUS can be used in the brain to elicit different bioeffects via thermal ablation[11], histotripsy[12–14], blood-brain barrier opening (BBBO) (drug-delivery, liquid biopsies)[15,16], hyperthermia (radiosensitization, enhanced local drug delivery)[17–19], sonodynamic therapy[20], and immunomodulation[21,22] as treatment for various brain pathologies. Typically, therapeutic systems in use have been optimized for a single FUS modality. The InSightec ExAblate® system uses a 650 kHz ultrasound array and is FDA approved to perform thermal ablation in central brain locations for essential tremor and Parkinsonian tremor. However, thermal ablation is limited to treat a small volume in the centre of the brain due to overheating of the skull[23,24]. A different 220 kHz ultrasound array is currently being used with the ExAblate® driving system in clinical trials to open the BBB and to perform neuromodulation[25–28]. However, neither the 650 kHz nor the 220 kHz ultrasound array is capable of performing mechanical ablation by histotripsy. Histotripsy uses cavitation to mechanically disrupt the target tissue and thus has the potential to treat a wider range of volumes and locations in the brain by mitigating skull heating using a very low duty cycle (< 0.1%)[29,30].

An All-in-One transcranial FUS system, that is capable of generating histotripsy, BBBO, hyperthermia, sonodynamic therapy, and immunomodulation in the murine brain, would be an enabling technology for FUS brain research for a wide range of brain locations and has not been available previously. Here we propose an All-in-One system that uses a single FUS transducer, the same driving electronics and is designed specifically for transcranial treatment in a murine brain, as most brain diseases models are available in mice. This All-in-One murine brain system is MR compatible to use with MRI-guidance and has stereotactic fiducial features to enable stereotactic treatment outside the MR scanner based on pre-treatment MR brain scans[31]. Such an All-in-One system with flexibility of MRI or stereotactic guidance enables testing the combination of different FUS

[1]Department of Biomedical Engineering, University of Michigan, Ann Arbor, MI, USA. [2]Department of Radiology, University of Michigan, Ann Arbor, MI, USA. [3]Department of Neurosurgery, University of Michigan, Ann Arbor, MI, USA. ✉email: taranak@umich.edu

modalities in the brain. A combination of different therapeutic modalities might be essential in treating certain brain pathologies. For example, to treat a brain tumor, histotripsy could first be used to debulk the central mass of a tumor and then sonodynamic therapy could be used to treat the infiltrative tumor margins. Additionally, modality comparison studies could be strengthened if the different modalities are performed using the same equipment by the same research group.

The parameters and instrumentation required for histotripsy is dramatically different from other modalities. Histotripsy uses microsecond-length, low duty cycle (< 0.1%), extremely high-pressure (> 26 MPa) ultrasound pulses[32,33], whereas hyperthermia uses continuous-wave (CW), lower-intensity ultrasound (100–300 W/cm^2)[34,35]. BBBO, sonodynamic therapy, and neuromodulation require parameters that are typically low pressure/intensity pulses of intermediate duty cycle[36–38]. This makes the design of a system capable of performing all these modalities in a single FUS system very challenging. The electronic driver has to be capable of producing high instantaneous voltage, but low time-averaged power required for histotripsy, as well as having sufficiently high electrical efficiency to sustainably produce CW ultrasound or longer tone bursts without overheating.

In this paper, an All-in-One FUS murine brain system was enabled by a "push-pull" electronic driver that is capable of producing a tone burst of any duration, ranging from extremely short pulses (a few cycles) at a peak-to-peak voltage of 1 kV required for histotripsy, or continuous waves (CW) at reduced voltage. A murine transcranial brain FUS transducer was designed and fabricated using the rapid prototyping method developed in our lab[39]. This All-in-One system can perform histotripsy and other FUS modalities using low-intensity continuous wave ultrasound or long ultrasound bursts.

The All-in-One system was designed to be MRI-compatible and fit inside an 80 mm imaging coil of a 7 Tesla small-animal MRI system allowing MR guidance and monitoring during hyperthermia treatment[40]. This system also contains stereotactic features to enable stereotactic targeting. For example, Histotripsy, BBBO, sonodynamic therapy and neuromodulation can be performed outside the MRI-scanner using stereotactic co-registration with pre-treatment MR-images. The dual guidance capabilities allow the most flexibility and can minimize MRI scanner time and cost for research as well as increasing throughput for treatment of subjects. This paper reports the design, fabrication, and acoustic characterization of this All-in-One FUS system and its testing in the murine naïve brain for histotripsy, BBBO, and hyperthermia treatments. The three modalities were chosen, because they cover the range of parameters (in terms of required duty cycle and voltage) for different FUS modalities.

Methods

System design and fabrication

Transducer design and fabrication

The therapy transducer was designed for preclinical studies in an *in-vivo* murine brain. Higher operating frequency allows for a smaller focal zone and more precise targeting. However, attenuation through the murine skull increases with frequency. Therefore, a resonant frequency of 1.5 MHz was chosen as a compromise point. The transducer consists of five 20 mm diameter flat elements arranged confocally at a distance of 25 mm. Each element is individually focused using a 3D printed lens for an effective total f-number of 0.61. The transducer has an effective aperture diameter of 41 mm and working distance of 3 mm. This allowed for the transducer to be small enough to fit inside an insert designed for an 80 mm imaging coil of a 7 Tesla small-animal MRI system (Agilent (Varian Inc., Pao Alto, CA)). The focal pressure estimated from the transducer was expected to have sufficient headroom for all the FUS modalities. To allow for ease of fabrication and minimize alignment error, the focusing lens for each element was integrated into a single combined scaffold.

The transducer structure with the integrated lenses was 3D printed using Somos PerFORM and elements were a hard porous ceramic PZT (PZ36, CTS, Kvistgård, Denmark) (Fig. 1). To bond each element to its lens inside the scaffold, a thin layer of epoxy (LOCTITE®, E-120HP (Hysol)) was used, and the elements were air-backed to maximize pressure output (due to no acoustic backpropagation). A 3D printed cap was used to make each element watertight. Four confocally orientated ports for needle hydrophones were accommodated in the

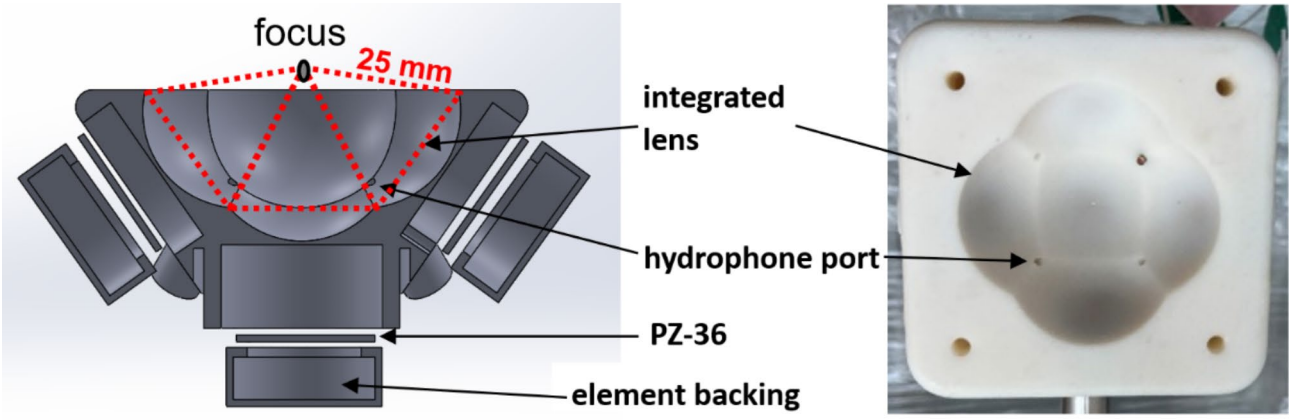

Fig. 1. Exploded cross-sectional drawing of the transducer's front view (left), top view photograph of the 3D printed scaffold (right).

transducer's scaffold to allow the collection of acoustic emissions during treatment. This includes the bubble nucleation and collapse emission signals during histotripsy, and sub-harmonic frequency signals caused by stable microbubble oscillation during BBBO.

To allow MRI guidance, the transducer was made to be MRI-compatible. The transducer element was comprised of lead zirconate titanate (PZT) with its electrodes made up of silver. The solder joint and wires from the PZT were made of non-ferrous materials. In addition to the entire scaffold, the MRI-insert, animal treatment holder, and platform were also 3D printed using MRI-safe resins manufactured by Formlabs (Somerville, Massachusetts, USA).

Supporting structures

For the animal experiments to be performed outside the MRI-scanner using stereotactic co-registration, a previously developed supporting structure design was used[31]. This included a 3D printed treatment bed with ear bars to rigidly mount the mouse head and two MR fiducials (Fig. 2a). The treatment bed was placed in the MRI scanner to acquire the pre-treatment images, then removed from the scanner and rigidly mounted on a platform fixed to the water tank (Envisionary Acrylics, Polk Country, Oregon) containing the transducer and degassed, deionized water. This platform had four holes corresponding to four removable pins on the transducer which was used to co-register the transducer to the fiducials on the treatment bed. The transducer was rigidly attached to a 3-axis positioning system (Anaheim Automation, Anaheim, California) which was used to mechanically steer it to the treatment coordinates after image-based calculations were made.

To demonstrate hyperthermia using MR-thermometry performed at the same time as sonication, an MRI-insert to accommodate the transducer and animal was developed (Fig. 2b). The transducer holder on the insert was positioned such that the focus would be at the iso-center of the 7 Tesla scanner. The same mouse treatment bed was used between the two treatment methods. A miniaturized platform on which the treatment bed was mounted allowed the transducer to target a single point in the cortex of the mouse's brain.

Driver design

The transducer was driven by in-house custom-built driving electronics. A 5-channel electronic driver was used to individually drive each element of the transducer, with the elements being pulsed simultaneously. Figure 3 shows a simplified schematic for a single channel, where the transducer was driven by semiconductor switches Q1 and Q2 operating in a "push-pull" configuration with a matching inductor to generate a sinewave output[41]. The switches were turned on and off at a frequency matching the resonant frequency of the transducer (1.5 MHz) and was controlled by a field-programmable gate array (FPGA). Based on its mode of operation, the same driver was able to produce a tone burst of any duration, ranging from extremely short pulses (a few cycles) at a peak-to-peak excitation voltage of 1 kV required for histotripsy, or continuous waves (CW) at reduced voltages of 20 V for hyperthermia. The excitation voltage to the transducer is adjusted by changing the voltage source, + Vdrive (from Fig. 3). For histotripsy, a 3-cycle pulse was used to allow the driver to ring up to the maximum corresponding excitation voltage. The components of the driver were selected to minimize RF noise and maximize CW efficiency and system output.

Acoustic characterization

The fabricated transducer was tested in free-field (FF) using a fiber optic hydrophone (HFO-690, Onda, Sunnyvale, CA, USA). The size of the transducer's focal zone was first measured. This was done by mounting the hydrophone to a 3-axis motor system, and raster scanning the pressure field of the transducer. For the lateral plane, a 2 × 2 mm field of view, centered at the focus, was measured using a resolution of 0.1 mm. For the axial plane, a 3 × 3 mm field of view, centered at the focus, was measured using a resolution of 0.1 mm.

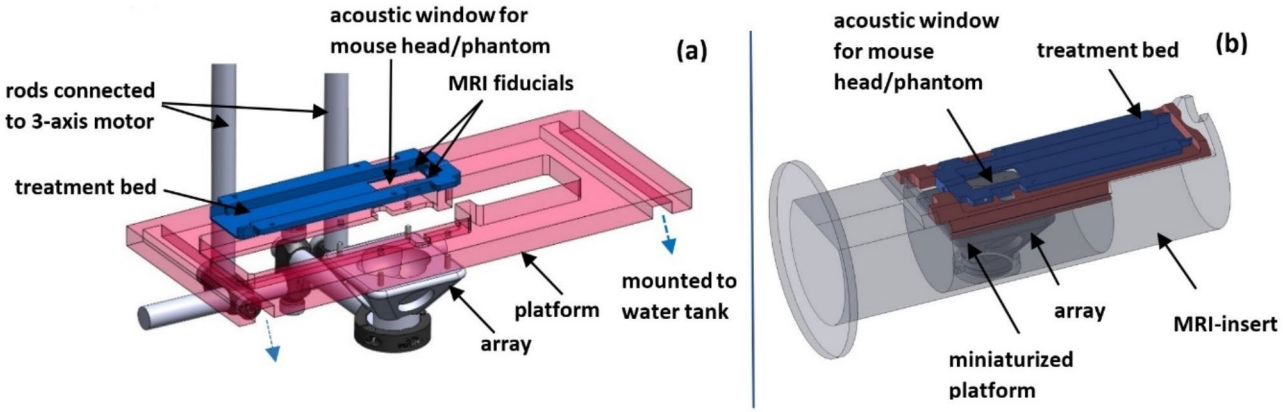

Fig. 2. CAD design of the supporting structures used for: MRI-based stereotactic co-registration of the transcranial treatments performed outside the MRI scanner (**A**); platform for transcranial treatments performed inside the MRI scanner (**B**).

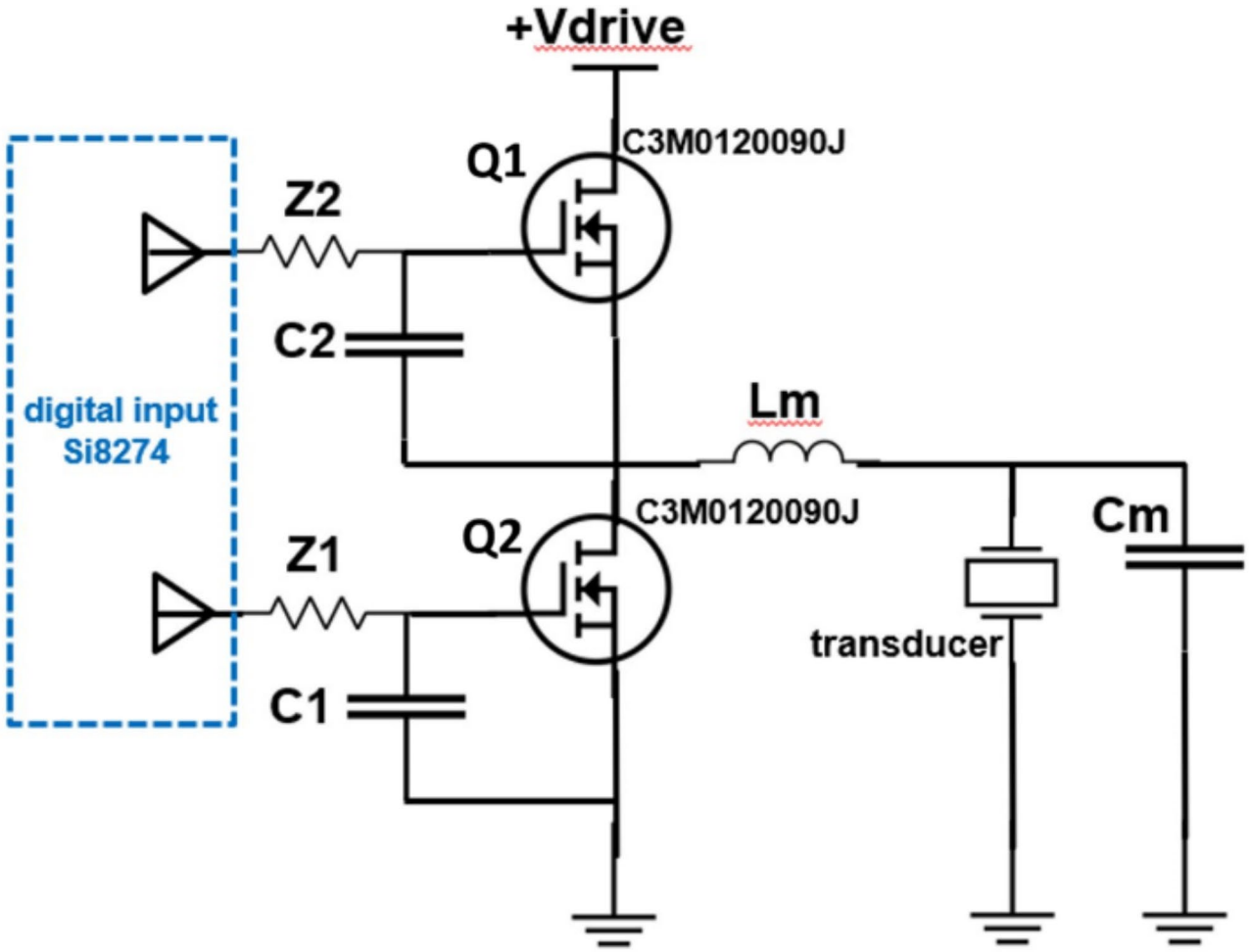

Fig. 3. Schematic of a single channel of the electronic driver. A pair of SiC transistors alternate sourcing and sinking current output to the transducer through an LC impedance matching circuit.

The pressure-temporal waveforms, peak pressures, spatial-peak temporal-average intensity (I_{spta}) required for histotripsy, hyperthermia and BBBO was also measured. These three applications of FUS were selected for testing because they cover the entire parameter space of all the FUS applications.

The driver was pulsed for a 7500-cycles (5 ms) burst at a pulse repetition frequency (PRF) of 5 Hz (2.5% duty cycle) for calibrating the BBBO mode, and 23-cycles (15 μs) at a PRF of 33.3 kHz (50% duty cycle) for hyperthermia mode. The voltage was linearly increased, and pressure from the entire transducer, pulsing all five elements simultaneously, was measured at its focus. The voltage was increased until either the driver started to get warm, the pressure output started to sag, or the current limit of the voltage source was reached. A duty cycle of 50% was used for hyperthermia mode instead of 100% to minimize off-target effects from standing waves generated within the mouse skull by true CW sonication.

The driver was then pulsed using 3-cycle pulses at a PRF of 10 Hz (0.002% duty cycle) for histotripsy mode calibration. The voltage was linearly increased, and focal pressure from the entire transducer was measured at levels below cavitation threshold. Above cavitation threshold, the corresponding pressure from each of the five elements at the focus was individually measured and then summed. This method of approximation was employed due to cavitation damage to the hydrophone tip when the entire transducer was pulsed above the cavitation threshold[42].

To estimate in-situ pressures, the attenuation through an excised mouse skull was measured. This was done by firing the transducer in histotripsy mode below cavitation threshold and measuring the focal pressure, first in free-field and then through the excised mouse skull.

In-vivo treatment

Histotripsy, BBBO, and hyperthermia were separately performed in two naïve mouse brains for each modality. These three FUS modalities were selected since they cover the entire FUS parameter space and involve treating outside (histotripsy and BBBO) and inside (hyperthermia) the MRI scanner. All animal procedures were carried out in accordance with protocol PRO00010789 as approved by the University of Michigan Institutional Animal Care & Use Committee. All methods are reported in accordance with the guidelines outlined in ARRIVE.

1. Histotripsy (n = 2)

Animal preparation and treatment setup: The C57BL/6 mouse was first anesthetized using isoflurane (1.5 mL/min) + oxygen (1 mL/min). The head of the mouse was shaved, and finer fur was removed using Nair cream with water. The head of the mouse was then affixed to the treatment bed (containing the MRI-fiducials) using ear bars, and the pre-treatment MRI-scans were taken. The animal was then placed on the treatment platform, and the transducer, in its home position, was co-registered to the left fiducial on the MRI-scans. The treatment location was demarcated on the target slice, and the corresponding motor coordinates were calculated. The transducer was then moved to these coordinates, and a single point lesion in the frontal cortex of the mouse's brain was created[31]. Motor-offsets of $-1.1 \times -0.25 \times -0.29$ mm (x, y, z) were used to account for aberration through the mouse skull based on prior experiments.

FUS parameters: A single focal location was targeted by 3-cycle ultrasound pulses, for 20 pulses at a 10 Hz PRF with an excitation voltage of 700 V (estimated *in-situ* peak-negative pressure of 45 MPa). Acoustic emissions from cavitation were passively received using a hydrophone in the transducer scaffold.

MRI scans used: MR images were acquired in a 60 mm birdcage coil. For detailed anatomical images pre- and post-treatment, T2-weighted images were acquired using a fast-spin echo sequence with the following parameters: 30 x 30 mm field of view, 0.5 mm slice thickness, 128 x 128 matrix, 0.23 mm pixel size, repetition time (TR) of 4000 ms, echo spacing (ESP) of 10 ms, effective echo time (TE) of 20 ms.

2. BBB Opening (BBBO) (n = 2)

Animal preparation and treatment setup: An awake C57BL/6 mouse was placed in a restraining device (Tail Vein Injector Platform, Braintree Scientific Inc., Massachusetts, USA). Lukewarm water was used to dilate the two lateral tail veins. An MLV-1 catheter (Braintree Scientific Inc., Massachusetts, USA) primed with heparin was then placed ~1.5 cm into one of the veins. This served as an access port for the microbubble injection prior to sonication. The mouse was then anesthetized using isoflurane (1.5 mL/min) + oxygen (1 mL/min). The same treatment setup and workflow as histotripsy for co-registration and target selection was followed. In this proof-of-concept study, two target points in the frontal cortex of the mouse's brain were selected for treatment in each subject.

Microbubble Preparation and Dosing: Microbubbles with a formulation similar to DEFINITY® (Lantheus Medical Imaging, Inc., Massachusetts, USA) were prepared in-house[43]. Each bubble consisted of a phospholipid sphere with a perfluoro butane core. On activation using VialMix® (Lantheus Medical Imaging, Inc., Massachusetts, USA), each vial had $(9.01 \pm 0.97) \times 10^9$ microbubbles with a mean diameter of 1.1 µm. The microbubbles were diluted in injectable saline using a dilution factor of 1:10. A bolus of 50–100 µl was injected through the tail vein catheter 1 min prior to sonication to allow for their systemic circulation.

FUS parameters: 2 treatment points were targeted in each mouse spaced by 1 mm. After an initial circulation period of 1 min, a 1 ms long ultrasound burst was applied at a PRF of 5 Hz for 30 s each at the two target locations. Between the two target sonications, a wait period of 1 min allowed for the recirculation of the microbubbles. An i*n-situ* pressure of 0.75 MPa was used.

MRI scans used: To obtain an anatomical image of the mouse's brain for pre-treatment lesion targeting, T2-weighted images were acquired. The parameters for the scan were the same as those used during histotripsy. To observe the BBBO post-treatment, Gadolinium (Gadoteridol, ProHance, 279.3 mg/ml) was injected through the peritoneum and T1-weighted images were acquired using a 30×30 mm field of view, 0.5 mm slice thickness, 128×128 matrix, 0.23 mm pixel size, repetition time (TR) of 1000 ms, echo spacing (SPE) of 7.95 ms, effective echo time (TE) of 7.95 ms. T2* images were acquired to check for vascular damage that may have occurred during treatment. The sequence involved a 30×30 mm field of view, 0.5 mm slice thickness, 128×128 matrix, 0.23 mm pixel size, repetition time (TR) of 230 ms, echo time (TE) of 5.5 ms.

3. Hyperthermia

Animal preparation and treatment setup: Similar to the histotripsy treatments, the C57BL/6 mouse was first anesthetized using isoflurane (1.5 mL/min) + oxygen (1 mL/min). The head of the mouse was shaved, and finer hair was removed using Nair cream with water. The head of the mouse was then affixed to the treatment bed using ear bars. This was then placed on the treatment platform which was subsequently placed on the MRI-insert containing the transducer in a degassed water bath. The entire system was then placed inside the 80 mm imaging coil which was in-turn placed inside the 7 Tesla MRI-scanner. A single point in the cortex of the mouse's brain was targeted.

At the end of the hyperthermia treatments, the mouse was kept anesthetized and euthanized using carbon dioxide overdose (flow rate: 1.5 L/min). The skullcap and underlying dura were checked for injury. The animal was anesthetized leading up to euthanasia to prevent any possible distress in case of injury due to excessive heat delivered to the skull or surface of the brain.

FUS parameters and MRI scans: A single point was targeted in the cortex of each mouse. Anatomical MR-images were first acquired. This involved a fast-spin echo T2 weighted axial image, with 96×69 mm field of view, 1 mm slice thickness, 192×96 matrix, repetition time (TR) of 2000 ms, echo time (TE) of 7.52 ms. To visualize heating and measure the focal temperature change, MR-thermometry images were acquired before, during and after sonication. RF -spoiled gradient echo images were acquired using a repetition time (TR) of 200 ms, and echo time (TE) of 6 ms, slice thickness of 1 mm, and in-plane spatial resolution of 0.6×0.7 mm. The resulted in a temporal resolution of 19.2 s. Subsequent phase images were subtracted from each other to get the change in temperature. The images were also corrected to accommodate for the temperature drift[44], and then zero-filled interpolated by a factor of 2. During sonication, a 15 µs long bursts of ultrasound was applied at a duty cycle of

50% with a resulting I_{spta} of 110 W/cm^2 for a total treatment duration of 2 min. A duty cycle of 50% was selected to minimize standing waves in the brain.

Results

Fabricated system and treatment setup

The transducer along with the electronic driver and supporting structures were successfully fabricated and assembled in-house. Figure 4a shows the fabricated transducer with the electronic driver. Figure 4b shows the in-vivo setup for the histotripsy and BBBO studies using MRI-based stereotactic co-registration. The mouse on its treatment bed is placed supine over the water tank containing the ultrasound transducer. The ultrasound transducer is rigidly attached to the 3-axis positioner. A MATLAB script is used to co-register the fiducials on the treatment bed to the transducer, select the target point, and fire the transducer.

Figure 4c shows the mouse placed on the MRI-insert for the hyperthermia studies. The MRI-insert contains the transducer placed in a water bath for acoustic coupling to the mouse's head. The MRI-insert is pictured next to the 80 mm imaging coil which in-turn is placed inside the bore of the 7 Tesla small animal MRI-scanner.

Acoustic characterization

The normalized 2D pressure field maps of the All-in-One FUS transducer measured by a fiber optic hydrophone are shown in Fig. 5. The field maps converted to x, y, z coordinates corresponded to the x axis being the direction of sound propagation, and the y and z axis perpendicular to it. yz was the coronal plane, and xy the axial plane in the MRI scanner. From the field maps acquired, the full-width half-maximum (FWHM) on the focal zone was $2 \times 0.6 \times 0.8$ mm (x, y, z).

For the output pressure calibration, Fig. 6a, b shows the increase in the focal peak-negative (P-) and peak-positive (P+) pressure with the increase in the voltage source (Vdrive). From the pressure-calibration, for 3-cycle histotripsy pulses, a maximum free-field focal P- of 85 MPa was estimated based on summation of measurements of the five elements individually.

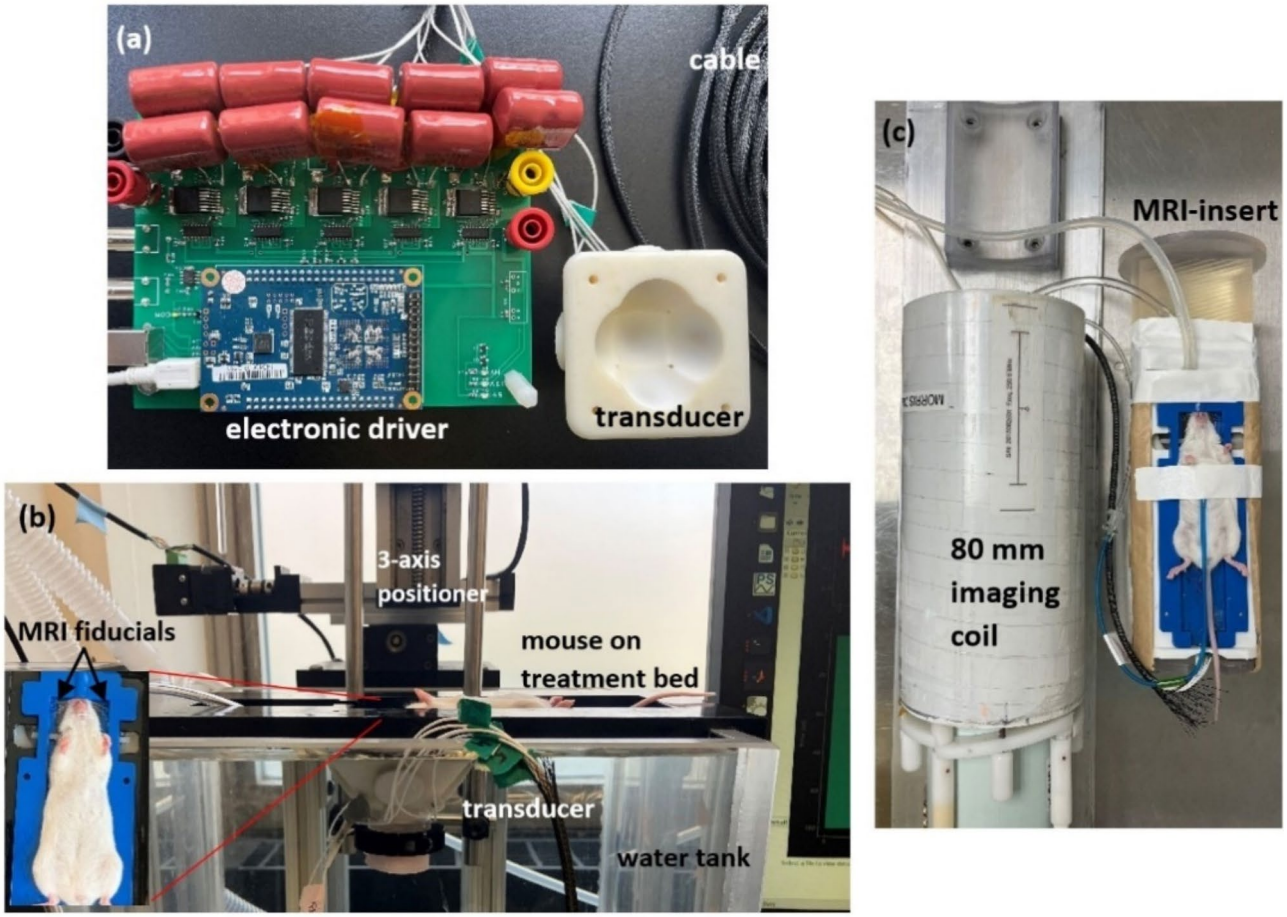

Fig. 4. Fabricated transducer and its electronic driver (**a**), in-vivo setup using MRI-based stereotactic-guidance used for histotripsy, BBBO treatments outside the MRI-scanner (**b**), *in-vivo* setup using MRI-guided treatment and monitoring for hyperthermia (**c**).

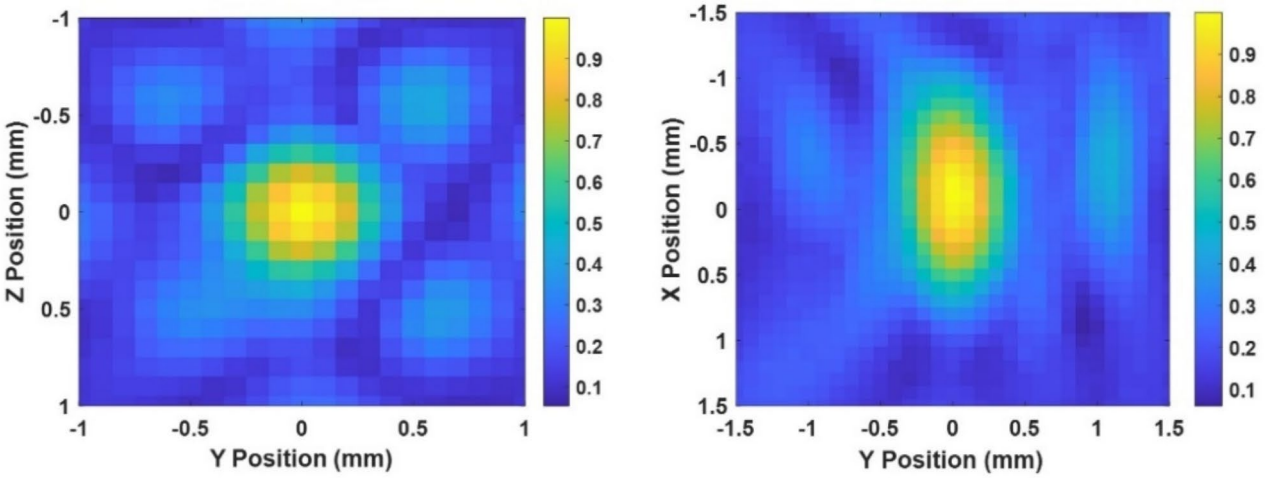

Fig. 5. Free-field lateral (left) and axial (right) field maps of the transducer.

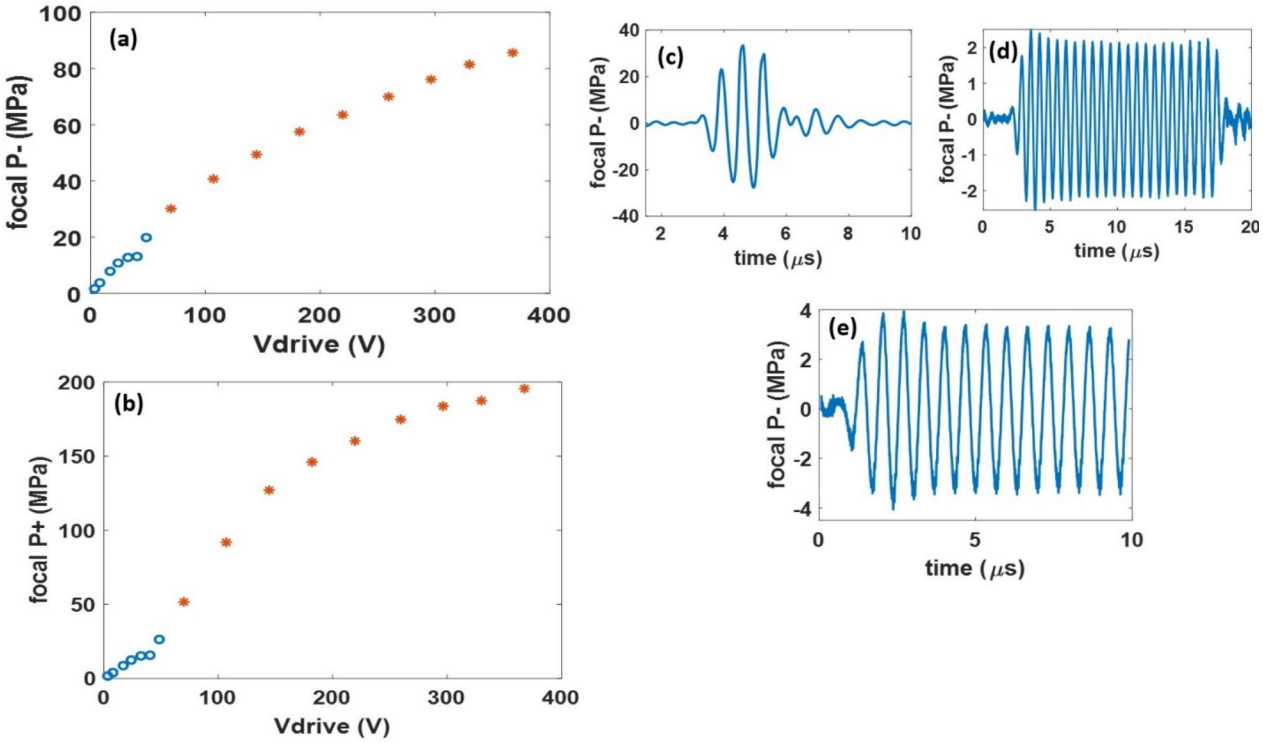

Fig. 6. Pressure-voltage curves of the transducer for the 3-cycle histotripsy pulses with the directly measured pressure values denoted by 'o's and the summed pressure values denoted by '*'s (**a**, **b**). Representative pressure-temporal waveforms for histotripsy (**c**), hyperthermia (**d**) & BBBO (**e**).

For the 5 ms ultrasound burst required for BBBO, a maximum pressure of 5.5 MPa before the current limit of the voltage source was reached. For similar burst durations, a pressure less than 1 MPa is used for stable cavitation of the microbubbles required to open the BBB with no vascular damage[45].

In hyperthermia mode (15 μs, 50% duty cycle pulse), the transducer produced a maximum P- of 4.5 MPa corresponding to an I_{spta} of 251 W/cm^2. For all three modalities, the driver was not warm to the touch, and no sag was seen in the pressure output of the transducer during a testing period of 15 min.

The attenuation through a mouse skull was measured to be 35%. Therefore, the transducer has sufficient acoustic headroom of 56 MPa for histotripsy, 4 MPa for BBBO, and 3 MPa for hyperthermia available in-situ. Figure 6c, d and e show representative measured pressure waveforms for the three FUS modalities.

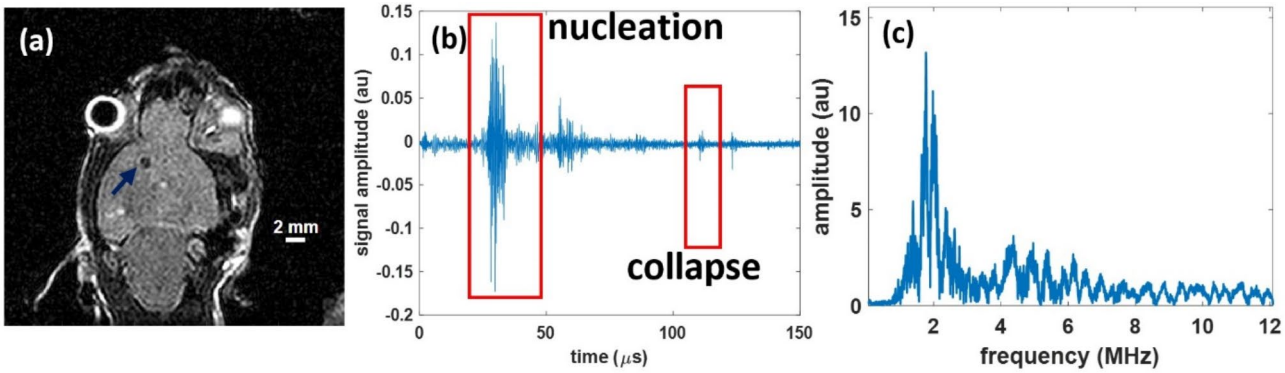

Fig. 7. The representative histotripsy lesion, viewed in a T2-w sagittal MR-image as a hypointense region (blue arrow) (**a**), and the hydrophone acoustic receive signals in the time showing signals corresponding to the bubble nucleation and subsequent collapse (**b**) and broadband signals in the frequency domain conducive with inertial cavitation (**c**).

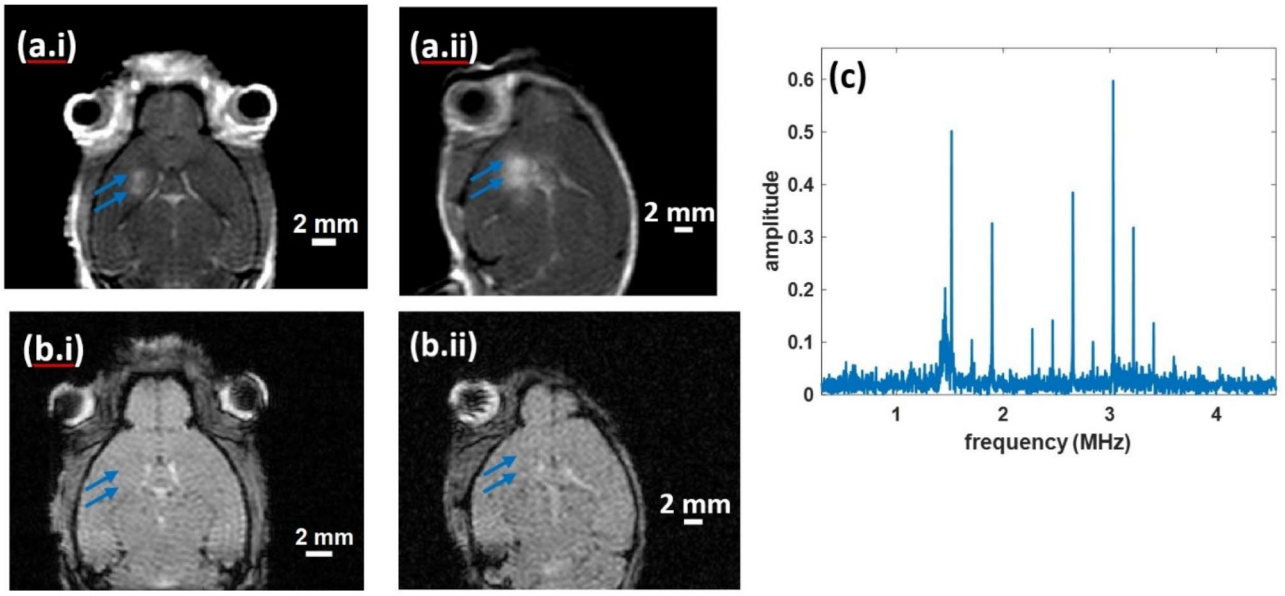

Fig. 8. T1-weighted Gd-enhanced images showing two focal regions of BBBO corresponding to the two targeted locations (blue arrows) (**a**), T2* images showing no hypointense regions of bleeding/edema (blue arrows) (**b**), hydrophone signal showing stable cavitation (**c**).

In-vivo treatment

Histotripsy

Successful histotripsy-ablated lesions were generated in the two naïve mouse brains. In the post-treatment coronal T2-weighted MR-image, the histotripsy-generated lesion was confirmed as a hypointense region (Fig. 7a). For the two mice the lesion sizes were measured from these hypointense regions in the MR-images and were $0.82 \times 0.88 \times 1$ mm, and $0.76 \times 0.93 \times 1$ mm, respectively. The targeting error (in x,y,z) was measured as the difference between the coordinates of the target zone in the pre-treatment image and the centroid of the lesion in the post-treatment image and was $0 \times 0.2 \times 0.11$ mm, and $-0.51 \times 0.21 \times 0.4$ mm, respectively.

Acoustic cavitation emission signals[46] received by the pin hydrophone showed nucleation and collapse signals in the time domain (Fig. 7.b), and broadband signals in the frequency domain (Fig. 7c), confirming successful in-situ inertial cavitation generation for every pulse with a bubble lifespan (time between cavitation nucleation and collapse signals) of 74.9 ± 8.1 μs.

BBB opening (BBBO)

Successful BBBO was achieved in the two mice tested and confirmed by MRI. For both, T1w Gd-enhanced images showed two regions of focal enhancement corresponding to the two target locations (Fig. 8ai and aii). The targeting error was $-1.38 \times -1.34 \times 0$ mm and $-0.78 \times 0.17 \times 0$ mm across the 2 animal treatments. No

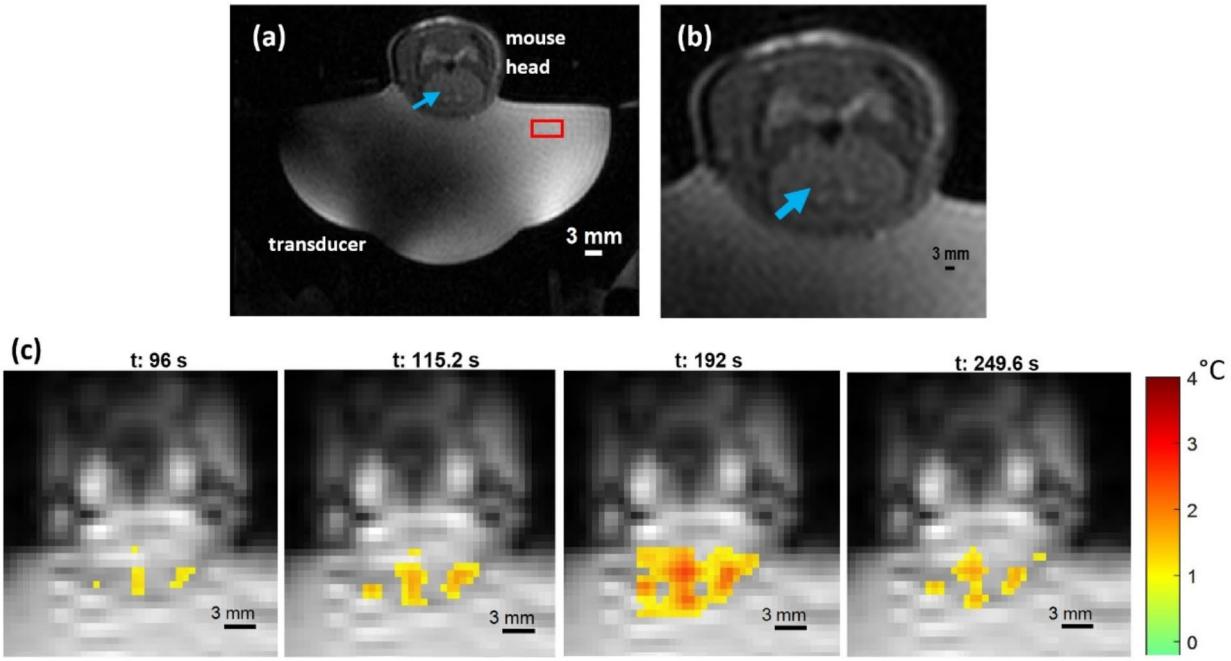

Fig. 9. Anatomical T2w MR-image showing the entire setup inside the scanner (**a**). The mouse brain with the target location (blue arrow) shown in the T2w image. MR-thermometry (gradient-echo) images right when the ultrasound is turned on (t = 96 s), when the heating reaches its peak (t = 192 s), and 1 min after the ultrasound is turned off (t = 249.6 s).

corresponding hypointense regions were seen in the T2* images (Fig. 8bi and bii) indicating no bleeding/edema. The absence of a broadband response and presence of harmonics in the frequency domain of the acoustic cavitation emission signals were consistent with stable cavitation of the circulating microbubbles during the application of ultrasound (Fig. 8c).

Hyperthermia

In each of the two mice, a focal heating zone corresponding to a temperature rise of 2.6 °C and 3.2 °C was observed. The in-plane spatial noise floor in the resulting thermometry images, measured at the 10th time point (115 s after the ultrasound was turned on), as the standard deviation in a 10 × 10-pixel square in the water bath (red box in Fig. 9a), was 0.124 °C and 0.09 °C in the two mice, respectively. Figure 9a and b visualizes the treatment setup including the target location (blue arrow), for a representative mouse. The evolution of the focal heating and subsequent cooling in the mouse brain is shown in Fig. 9c – the moment the transducer was turned on, during sonication, and after the transducer was turned off. Heating of the skull's surface (off-target) was also observed due to its proximity to the targeted location. 28 ± 4 voxels surrounding the target location reached 50% of the peak temperature and 22 ± 11 voxels at all the off-target locations reached similar temperatures. Additionally, the ratio of peak temperature off-target to that at the target location was measured to be 1.11 ± 0.25. On gross dissection, no signs of injury due to delivery of excessive thermal energy were observed on the underlying cortex, dura, or the surface of the skull.

Discussion

In this paper a single FUS transducer, consisting of 5 elements, and electronic driver was shown to be capable of producing microsecond-long bursts of a thousand volts necessary for histotripsy as well as CW ultrasound or long ultrasound pulses at low to intermediate pressure for BBBO and hyperthermia. The system can use either MRI guidance or stereotactic guidance for treatment targeting, allowing for the increased flexibility of using it. The system was successfully validated in a murine brain for histotripsy, hyperthermia and BBBO. Since neuromodulation or sonodynamic therapy requires pulses with a burst duration similar to BBBO but pressure values in the lower kilo-Pascal range[33,35], the system is expected to capable of performing these modalities as well. This allows for the exploration of certain brain pathologies to be treated using a combination of therapies. For example, brain tumors like glioblastoma multiforme are highly aggressive and is accompanied by a poor overall survival rate[47]. Single modality treatments have shown limited success in improving the outcomes of these patients[48]. The development of such a system can open avenues of exploring multiple modality-based treatments with the potential of improving survival outcomes. It is worth noting that although the system is expected to be capable of inducing neuromodulation, *in-vivo* validation is required since there is still a degree of variation in treatment parameters required for the implementation and success within the field of FUS neuromodulation.

This system was not designed to use thermal ablation as one of the FUS modalities. Thermal ablation is restricted to treating small *in-vivo* volumes due to the heat sink effect that tissues possess. This would especially be a challenge when treating highly vascularized tumors in the brain. Additionally, thermal ablation cannot be used to treat structures closer to the skull due to significantly increased risk of overheating the skull. Thermal ablation requires a higher time-averaged intensity, the pulsing parameters of which would put a considerable thermal strain on both the transducer as well as the electronic driver.

For histotripsy, the acoustic emission signals from the cavitation bubble cloud's formation and collapse can be used for monitoring, and subsequently can be a good predictor of successful treatment before the post-treatment MR-images are acquired. Being a broadband receiver, the pin hydrophones are also capable of detecting harmonic frequencies indicative of stable cavitation of the microbubbles injected in a mouse when ultrasound is applied for successful BBBO. It can also be used to detect the presence of wideband signals produced by microbubble fractionation during undesirable inertial cavitation[49,50] for FUS modalities like BBBO, sonodynamic therapy or neuromodulation.

The transducer was fabricated using 3D printing resins like PerFORM that are MRI-compatible. However, there were considerable distortions in the field from the PZT electrodes as seen in Fig. 9a. Since the mouse brain and focal zone were not obscured by these distortions, they were not corrected for.

For MRI-guided hyperthermia treatment, a single focal heating zone was created for the first proof-of-concept experiments. To reach the desired hyperthermia temperature in a murine brain, the ultrasound only had to be turned on for 2 min. This duration is much shorter than that of clinically-relevant hyperthermia[51], in which the therapeutic effects of hyperthermia are achieved by maintaining the target region at a minimum of 43 °C for 10–15 min[52]. This treatment effect translates pre-clinically as well, therefore, longer-duration hyperthermia studies may require additional measures to mitigate off-target skull heating. To do this, circulating cooling water can be used in the water bath as a heat sink to prevent the accumulation of heat at the skull. To be able to steer the focus with the transducer inside the MRI-scanner, a 3D MRI-compatible motorized positioner would be needed, since the motorized positioner used for stereotactic targeting is not MRI-compatible. Adding MRI-compatible motors would allow all the modalities for volume treatment to be performed inside the scanner, and benefit from MRI monitoring tools like real-time MRI detection of cavitation[53], diffusion weighted imaging (DWI), etc. However, the cost of the system would significantly increase. Additionally, the 5-element transducer cannot perform aberration correction. The absence of aberration correction was not seen to significantly affect the in-vivo targeting accuracy for murine brain studies. However, a phased array with a higher element count can be built to perform aberration correction.

Conclusion

This study developed the first pre-clinical transcranial All-in-One FUS system capable of performing histotripsy, hyperthermia, BBBO, sonodynamic therapy and neuromodulation in-vivo in a murine brain. A 1.5 MHz, 5 element transducer and a "pushand- pull" electronic driver were designed and fabricated. The transducer was characterized in free field, producing microsecond-length pulses with a P- of 85 MPa, and CW pulses (50% duty cycle) with an Ispta of 251 W/cm2. The attenuation through an excised mouse skull was measured at ~35% demonstrating sufficient headroom, without aberration correction, for the system to be able to perform the above-mentioned modalities, non invasively in a murine brain. This All-in-One system can be used both with MRI guidance and stereotactic targeting to maximize its flexibility. Successful histotripsy, BBBO, and hyperthermia treatments were carried out separately in the brains of naïve mice demonstrating the ability of the system to perform the modalities across the FUS parameter space. These results demonstrate the ability of this transcranial All-in-One FUS system to be used in exploring individual or combination therapies pre-clinically for different brain pathologies in murine models.

Data availability

Data is provided within the paper itself.

Received: 12 September 2024; Accepted: 19 December 2024
Published online: 02 January 2025

References

1. Hersh, D. S. et al. Emerging applications of therapeutic ultrasound in neuro-oncology: moving beyond tumor ablation. *Neurosurgery* **79**(5), 643–654. https://doi.org/10.1227/NEU.0000000000001399 (2016).
2. Roberts, J. W., Powlovich, L., Sheybani, N. & LeBlang, S. Focused ultrasound for the treatment of glioblastoma. *J. Neuro-Oncol.* **157**(2), 237–247. https://doi.org/10.1007/s11060-022-03974-0 (2022).
3. Gerhardson, T. *Transcranial Therapy for Intracerebral Hemorrhage and Other Brain Pathologies using Histotripsy* (2020).
4. Alptekin, A. et al. Pulsed focal ultrasound as a non-invasive method to deliver exosomes in the brain/stroke. *J. Biomed. Nanotechnol.* **17**(6), 1170–1183. https://doi.org/10.1166/jbn.2021.3091 (2021).
5. Ahmed, A. K. et al. Technical comparison of treatment efficiency of magnetic resonance-guided focused ultrasound thalamotomy and pallidotomy in skull density ratio-matched patient cohorts. *Front. Neurol.* **21**(12), 808810. https://doi.org/10.3389/fneur.2021.808810 (2022).
6. Sammartino, F., Yeh, F. C. & Krishna, V. Intraoperative lesion characterization after focused ultrasound thalamotomy. *J. Neurosurg.* **31**, 1–9 (2021).
7. Moosa, S. et al. The role of high-intensity focused ultrasound as a symptomatic treatment for Parkinson's disease. *Mov. Disord.* **34**, 1243–1251. https://doi.org/10.1002/mds.27779 (2019).
8. Jeong, H. et al. Short-term efficacy of transcranial focused ultrasound to the hippocampus in Alzheimer's disease: A preliminary study. *J. Pers. Med.* **12**(2), 250. https://doi.org/10.3390/jpm12020250 (2022).
9. Epelbaum, S. et al. Pilot study of repeated blood-brain barrier disruption in patients with mild Alzheimer's disease with an implantable ultrasound device. *Alzheimers Res. Ther.* **14**(1), 40. https://doi.org/10.1186/s13195-022-00981-1 (2022).

10. Dubey, S. et al. Clinically approved IVIg delivered to the hippocampus with focused ultrasound promotes neurogenesis in a model of Alzheimer's disease. *Proc. Natl. Acad. Sci. U. S. A.* **117**(51), 32691–32700. https://doi.org/10.1073/pnas.1908658117 (2020).
11. Izadifar, Z., Izadifar, Z., Chapman, D. & Babyn, P. An Introduction to high intensity focused ultrasound: Systematic review on principles, devices, and clinical applications. *J. Clin. Med.* **9**(2), 460. https://doi.org/10.3390/jcm9020460 (2020).
12. Xu, Z. et al. Controlled ultrasound tissue erosion. In *Proceedings of the IEEE Ultrasonics Symposium* vol. 1, 732–735 (2003).
13. Duclos, S., Golin, A., Fox, A., Chaudhary, N., Camelo-Piragua, S., Pandey, A., & Xu, Z. Transcranial histotripsy parameter study in primary and metastatic murine brain tumor models. *Int. J. Hyperth.* **40**(1). https://doi.org/10.1080/02656736.2023.2237218. (2023)
14. Duclos, S. et al. Characterization of blood-brain barrier opening induced by transcranial histotripsy in murine brains. *Ultrasound Med. Biol.* **50**(5), 639–646. https://doi.org/10.1016/j.ultrasmedbio.2023.12.014 (2024).
15. Burgess, A., Shah, K., Hough, O. & Hynynen, K. Focused ultrasound-mediated drug delivery through the blood-brain barrier. *Expert. Rev. Neurother.* **15**(5), 477–491. https://doi.org/10.1586/14737175.2015.1028369 (2015).
16. Meng, Y. et al. MR-guided focused ultrasound liquid biopsy enriches circulating biomarkers in patients with brain tumors. *Neuro Oncol.* **23**(10), 1789–1797. https://doi.org/10.1093/neuonc/noab057 (2021).
17. Zhu, L. et al. Ultrasound hyperthermia technology for radiosensitization. *Ultrasound Med. Biol.* **45**(5), 1025–1043. https://doi.org/10.1016/j.ultrasmedbio.2018.12.007 (2019).
18. Datta, N. R. et al. Local hyperthermia combined with radiotherapy and-/or chemotherapy: Recent advances and promises for the future. *Cancer Treat Rev.* **41**(9), 742–753. https://doi.org/10.1016/j.ctrv.2015.05.009 (2015).
19. Gray, M. D. et al. Focused ultrasound hyperthermia for targeted drug release from thermosensitive liposomes: results from a phase I trial. *Radiology* **291**(1), 232–238. https://doi.org/10.1148/radiol.2018181445 (2019).
20. Tachibana, K., Feril, L. B. Jr. & Ikeda-Dantsuji, Y. Sonodynamic therapy. *Ultrasonics.* **48**(4), 253–259. https://doi.org/10.1016/j.ultras.2008.02.003 (2008).
21. Chen, P. Y. et al. Focused ultrasound-induced blood-brain barrier opening to enhance interleukin-12 delivery for brain tumor immunotherapy: A preclinical feasibility study. *J. Transl. Med.* **13**, 93. https://doi.org/10.1186/s12967-015-0451-y (2015).
22. Cohen-Inbar, O., Xu, Z. & Sheehan, J. P. Focused ultrasound-aided immunomodulation in glioblastoma multiforme: A therapeutic concept. *J. Ther. Ultrasound.* **22**(4), 2. https://doi.org/10.1186/s40349-016-0046-y (2016).
23. McDannold, N., Clement, G., Black, P., Jolesz, F. A. & Hynynen, K. Transcranial MRI-guided focused ultrasound surgery of brain tumors: Initial findings in three patients. *Neurosurgery* **66**(2), 323–332. https://doi.org/10.1227/01.NEU.0000360379.95800.2F.Transcranial (2010).
24. Arvanitis, C. D., Vykhodtseva, N., Jolesz, F., Livingstone, M. & McDannold, N. Cavitation-enhanced nonthermal ablation in deep brain targets: Feasibility in a large animal model. *J. Neurosurg.* **124**(5), 1450–1459. https://doi.org/10.3171/2015.4.JNS142862 (2016).
25. Morabito, R. et al. The role of treatment-related parameters and brain morphology in the lesion volume of magnetic-resonance-guided focused ultrasound thalamotomy in patients with tremor-dominant neurological conditions. *Bioengineering* **11**(4), 373 (2024).
26. Bancel, T. et al. Sustained reduction of essential tremor with low-power non-thermal transcranial focused ultrasound stimulations in humans. *Brain Stimul.* **17**(3), 636–647 (2024).
27. D'Haese, P. F. et al. β-amyloid plaque reduction in the hippocampus after focused ultrasound-induced blood–brain barrier opening in Alzheimer's disease. *Front. Hum. Neurosci.* **14**, 593672 (2020).
28. Park, S. H. et al. Safety and feasibility of multiple blood-brain barrier disruptions for the treatment of glioblastoma in patients undergoing standard adjuvant chemotherapy. *J. Neurosurg.* **134**(2), 475–483 (2020).
29. Gerhardson, T. et al. Effect of frequency and focal spacing on transcranial histotripsy clot liquefaction, using electronic focal steering. *Ultrasound Med. Biol.* **43**(10), 2302–2317. https://doi.org/10.1016/j.ultrasmedbio.2017.06.010 (2017).
30. Lu, N. et al. Transcranial MR-guided histotripsy system. *IEEE Trans. Ultrason. Ferroelectr. Freq. Control.* https://doi.org/10.1109/TUFFC.2021.3068113 (2021).
31. Choi, S. W. et al. Stereotactic transcranial focused ultrasound targeting system for murine brain models. *IEEE Trans. Ultrason. Ferroelectr. Freq. Control* **68**(1), 154–163. https://doi.org/10.1109/TUFFC.2020.3012303 (2021).
32. Maxwell, A. D., Cain, C. A., Hall, T. L., Fowlkes, J. B. & Xu, Z. Probability of cavitation for single ultrasound pulses applied to tissues and tissue-mimicking materials. *Ultrasound Med. Biol.* **39**(3), 449–465. https://doi.org/10.1016/j.ultrasmedbio.2012.09.004 (2013).
33. Gateau, J. et al. In vivo bubble nucleation probability in sheep brain tissue. *Phys. Med. Biol.* **56**(22), 7001–7015. https://doi.org/10.1088/0031-9155/56/22/001 (2011).
34. Partanen, A. et al. Mild hyperthermia with magnetic resonance-guided high-intensity focused ultrasound for applications in drug delivery. *Int J Hyperthermia.* **28**(4), 320–336. https://doi.org/10.3109/02656736.2012.680173 (2012) (**Erratum in: Int J Hyperthermia. 2012;28(5):473**).
35. Guillemin, P. C. et al. Mild hyperthermia by MR-guided focused ultrasound in an ex vivo model of osteolytic bone tumour: Optimization of the spatio-temporal control of the delivered temperature. *J. Transl. Med.* **17**(1). https://doi.org/10.1186/s12967-019-2094-x (2019).
36. Raspagliesi, L. et al. Intracranial sonodynamic therapy with 5-aminolevulinic acid and sodium fluorescein: Safety study in a porcine model. *Front. Oncol.* **21**(11), 679989. https://doi.org/10.3389/fonc.2021.679989 (2021).
37. Lapin, N. A., Gill, K., Shah, B. R., & Chopra, R. Consistent opening of the blood brain barrier using focused ultrasound with constant intravenous infusion of microbubble agent. *Sci. Rep.* **10**(1). https://doi.org/10.1038/s41598-020-73312-9. (2020)
38. Focused Ultrasound Foundation. *Neuromodulation Workshop* (2014).
39. Kim, Y. et al. Rapid prototyping fabrication of focused ultrasound transducers. *IEEE Trans. Ultrason. Ferroelectr. Freq. Control* **61**(9), 1559–1574. https://doi.org/10.1109/TUFFC.2014.3070 (2014).
40. O'Neill, B. E., Karmonik, C., Sassaroli, E. & Li, K. C. Estimation of thermal dose from MR thermometry during application of nonablative pulsed high intensity focused ultrasound. *J. Magn. Reson. Imaging* **35**(5), 1169–1178. https://doi.org/10.1002/jmri.23526 (2012).
41. Umemura, S. I. & Cain, C. A. Acoustical evaluation of a prototype sector-vortex phased-array applicator. *IEEE Trans. Ultrason. Ferroelectr. Freq. Control* **39**(1), 32–38 (1992).
42. Vlaisavljevich, E. et al. Histotripsy-induced cavitation cloud initiation thresholds in tissues of different mechanical properties. *IEEE Trans. Ultrason. Ferroelectr. Freq. Control* **61**(2), 341–352. https://doi.org/10.1109/TUFFC.2014.6722618 (2014).
43. Kalayeh, K. et al. Ultrasound contrast stability for urinary bladder pressure measurement. *Ultrasound Med. Biol.* **49**(1), 136–151. https://doi.org/10.1016/j.ultrasmedbio.2022.08.008 (2023).
44. Rieke, V. et al. Referenceless PRF shift thermometry. *Magn. Reson. Med.* **51**(6), 1223–1231. https://doi.org/10.1002/mrm.20090 (2004).
45. Konofagou, E. E. Optimization of the ultrasound-induced blood-brain barrier opening. *Theranostics* **2**(12), 1223–1237. https://doi.org/10.7150/thno.5576 (2012).
46. Yeats, E., Lu, N., Sukovich, J. R., Xu, Z. & Hall, T. L. Soft tissue aberration correction for histotripsy using acoustic emissions from cavitation cloud nucleation and collapse. *Ultrasound Med. Biol.* **49**(5), 1182–1193. https://doi.org/10.1016/j.ultrasmedbio.2023.01.004 (2023).
47. Krex, D. et al. for the German glioma network, long-term survival with glioblastoma multiforme. *Brain* **130**(10), 2596–2606. https://doi.org/10.1093/brain/awm204 (2007).

48. Hersh, A. M. et al. Applications of focused ultrasound for the treatment of glioblastoma: A new frontier. *Cancers* **14**(19), 4920. https://doi.org/10.3390/cancers14194920 (2022).
49. Yang, Y. et al. Cavitation dose painting for focused ultrasound-induced blood-brain barrier disruption. *Sci. Rep.* **9**, 2840. https://doi.org/10.1038/s41598-019-39090-9 (2019).
50. Chu, P. C. et al. Focused ultrasound-induced blood-brain barrier opening: association with mechanical index and cavitation index analyzed by dynamic contrast-enhanced magnetic-resonance imaging. *Sci. Rep.* **15**(6), 33264. https://doi.org/10.1038/srep33264 (2016).
51. Chan, H., Chang, H. Y., Lin, W. L. & Chen, G. S. Large-volume focused-ultrasound mild hyperthermia for improving blood-brain tumor barrier permeability application. *Pharmaceutics* **14**(10), 2012. https://doi.org/10.3390/pharmaceutics14102012 (2022).
52. Datta, N. R. et al. Local hyperthermia combined with radiotherapy and-/or chemotherapy: Recent advances and promises for the future. *Cancer Treat. Rev.* **41**(9), 742–753. https://doi.org/10.1016/j.ctrv.2015.05.009 (2015).
53. Allen, S. & Hall, T. Real-time MRI feedback of cavitation ablation therapy (histotripsy). *J. Ther. Ultrasound* **3**(Suppl 1), O89. https://doi.org/10.1186/2050-5736-3-S1-O89 (2015).

Acknowledgements

This research was supported by a grant from the Focused Ultrasound Foundation. Drs. Jonathan Sukovich, Zhen Xu, Timothy L. Hall, and University of Michigan have conflict of interests with HistoSonics. The remaining authors do not any conflicts of interest.

Author contributions

The manuscript involved a collaborative effort by ten co-authors, and each author's contribution to the work is stated as follows: Tarana Parvez Kaovasia, Timothy Hall, Zhen Xu, Jonathan Sukovich, Aditya Pandey and Douglas Noll conceived and designed the analysis. Kourosh Kalayeh and Mario Fabiilli prepared the microbubbles and accompanying expertise in performing the experiments. Tarana Parvez Kaovasia, Sarah Duclos and Dinank Gupta collected the data. Tarana Parvez Kaovasia and Dinank Gupta performed analysis of the data. All authors discussed the results, contributed to the final manuscript, and approved the final version of the manuscript for submission.

Competing interests

Drs. Jonathan Sukovich, Zhen Xu, Timothy L. Hall, and University of Michigan have conflict of interests with HistoSonics. The remaining authors do not any conflicts of interest.

Additional information

Supplementary Information The online version contains supplementary material available at https://doi.org/10.1038/s41598-024-84078-9.

Correspondence and requests for materials should be addressed to T.P.K.